Published in final edited form as:

Oncogene. 2014 December 11; 33(50): 5688–5696. doi:10.1038/onc.2013.507.

Mechanism of Human PTEN Localization Revealed by Heterologous Expression in *Dictyostelium*

Hoai-Nghia Nguyen, **Yashar Afkari**, **Hiroshi Senoo**, **Hiromi Sesaki**, **Peter N. Devreotes***, and **Miho Iijima***

Department of Cell Biology, The Johns Hopkins University School of Medicine, Baltimore, MD

Abstract

Phosphatase and tensin homolog (PTEN) is one of the most frequently mutated tumor suppressor genes in cancers. PTEN plays a central role in phosphatidylinositol (3,4,5)-trisphosphate (PIP3) signaling and converts PIP3 to phosphatidylinositol (4,5)-bisphosphate (PIP2) at the plasma membrane. Despite its importance, the mechanism that mediates membrane localization of PTEN is poorly understood. Here, we generated a library that contains GFP fused to randomly mutated human PTEN and expressed the library in *Dictyostelium* cells. Using live cell imaging, we identified mutations that enhance the association of PTEN with the plasma membrane. These mutations were located in four separate regions, including the phosphatase catalytic site, the calcium-binding region 3 (CBR3) loop, the Cα2 loop and the C-terminal tail phosphorylation site. The phosphatase catalytic site, the CBR3 loop and the Cα2 loop formed the membrane-binding regulatory interface and interacted with the inhibitory phosphorylated C-terminal tail. Furthermore, we showed that membrane recruitment of PTEN is required for PTEN function in cells. Thus, heterologous expression system in *Dictyostelium* cells provides mechanistic and functional insight into membrane localization of PTEN.

Keywords

PTEN; Membrane localization; Mutational analysis; *Dictyostelium*

Introduction

Excessive PIP3 signaling caused by alternations in PI3K, PTEN or the PIP3-regualted serine/threonine kinase AKT leads to tumor formation and metastasis (1-3). While PI3K inhibitors have been developed as anti-cancer drugs to suppress PIP3 production (4, 5), activators of PTEN have not been explored. Despite the central role of PTEN in PIP3 signaling at the plasma membrane, the majority of PTEN is present in the cytosol and nucleus (6, 7). Stimulating membrane localization of PTEN could potentially enhance its tumor suppressor function. Currnetly, the details of the mechanism of membrane localization are unclear.

*Correspondence: miijima@jhmi.edu, pnd@jhmi.edu.

PTEN has four distinct domains; an N-terminal lipid binding domain (LBD), phosphatase domain, C2 domain, and C-terminal tail domain (Fig. 1A) (7, 8). The lipid binding, phosphatase and C2 domains can interact with phospholipids *in vitro* (9-11). While the 3-D structure of the phosphatase and C2 domains of PTEN has been revealed, the structure of the tail domain is not solved and proposed to be a flexible fragment (12). The C-terminal tail binds the other part of PTEN and blocks its membrane association. This inhibitory, intramolecular interaction requires phosphorylation at S380, T382, T383 and S385 in the tail. When these residues were substituted with alanine ($PTEN_{A4}$), increased association with the plasma membrane and nucleus were observed in cells (9, 13). In this study, we developed a heterologous expression system, in which human PTEN-GFP was expressed in *Dictyostelium* cells. Human PTEN is functional in *Dictyostelium* cells, as it rescues PTEN-null phenotypes (14-17). Using the powerful genetic system and accessible imaging of membrane localization afforded by expression in *Dictyostelium*, we defined the mechanism and regulation of human PTEN localization.

Results

Human PTEN-GFP is mainly located in the cytosol of mammalian and *Dictyostelium* cells (9, 15). We used error-prone PCR to generate a library of randomly mutated human PTEN cDNAs fused to GFP (complexity = 120,000, average mutation rate = 5.5 per molecule) and transfected the library into PTEN-null *Dictyostelium* cells. After selecting transformants in the presence of the antibiotic geneticin, we visually inspected ~20,000 colonies and collected 18 colonies that showed increased membrane association of PTEN-GFP (Fig. 1A). After isolation of plasmids and DNA sequencing, the mutations were separated and re-examined for their effects on PTEN localization in *Dictyostelium* cells. Demonstrating the feasibility of our screen, we isolated mutations that have been reported to enhance membrane localization of PTEN (Fig. 1A-C) (9, 15). These mutations were located in the catalytic site (cysteine at amino acid residue 124 changed to arginine or serine, C124R/S) and in the C-terminal region that spans phosphorylation sites (amino acid residues 380-385). The C-terminal mutations also increased nuclear localization. Combinations of C124R/S with the C-terminal mutations further increased membrane localization (Fig. 1A-C), as previously described (13).

It has been shown that phosphorylation of the C-terminal tail is important for the stability of PTEN (18). To examine the role of PTEN stability in its localization, we treated cells expressing either $PTEN_{A4}$, in which phosphorylation sites S380, T382, T383, and S385 were mutated to alanine, with a proteasome inhibitor, MG132 (Fig. 1B-E). Intriguingly, membrane localization of $PTEN_{A4}$, but not its nuclear localization, was significantly enhanced. The localization of WT PTEN, which is mainly located in the cytosol, was not affected by MG132. Consistent with these microscopic observations, quantification of immunoblotting showed that MG132 treatments increased the total amount of $PTEN_{A4}$, but not WT PTEN (Fig. 1F). We then asked if increased membrane association of $PTEN_{C124S,A4}$ resulted from increased stability of $PTEN_{A4}$ by C124S. In contrast to $PTEN_{A4}$, membrane association of $PTEN_{C124S}$ and $PTEN_{C124S,A4}$ was not affected by MG132 (Fig. 1B and C).

To further examine the effect of C124S and C-terminal phosphorylation sites mutations on PTEN localization, we inhibited protein synthesis using cycloheximide. Membrane association of $PTEN_{A4}$ was selectively decreased by cycloheximide treatment and this decrease was rescued by C124S mutation (Fig. 1B and C). Similarly, $PTEN_{A4}$ showed a decreased half-life in the presence of cycloheximide and additional C124S mutation restored the normal protein stability (Fig. 1G). These results suggest that PTEN at the plasma membrane is more sensitive to proteasome-mediated degradation and the mutation C124S confers increased resistance.

Since C124 is required for the phosphatase activity of PTEN, we tested whether loss of catalytic activity stabilizes membrane association of $PTEN_{A4}$. Supporting this notion, another catalytic site mutation, R130G, also stabilized $PTEN_{A4}$ at the membrane in the absence of MG132 (Fig. 2A and B). However, in contrast to C124S, R130G alone did not increase membrane localization of PTEN. These data suggested that loss of phosphatase activity stabilizes membrane localization of $PTEN_{A4}$ but alone is not sufficient to target PTEN to the membrane.

Previous studies have suggested that $PTEN_{C124S}$ is a “substrate-trapping” mutant which forms a stable complex with PIP3 at the plasma membrane (19). This model predicts that the membrane localization of $PTEN_{C124S}$ depends on PIP3. To test the prediction, we treated cell with an inhibitor of PI3K, LY294002, which decreased PIP3 levels as shown by the loss of a PIP3 biosensor, PHcrac-GFP, from the plasma membrane (Fig. 2C and D). However, membrane association of $PTEN_{C124S}$ was not affected in LY294002-treated cells (Fig. 2C and D). Similarly, membrane localization of $PTEN_{C124S}$ was not affected in PTEN-null cells in which PIP3 levels are increased (Fig. 2C and D). These results suggest that membrane association of $PTEN_{C124S}$ is independent of PIP3.

To explore whether, C124S has an additional role in membrane targeting, we examined interactions of PTEN with the C-terminal tail in pull-down assays (Fig. 2E-G) (9). In this assay, we expressed full length PTEN as a GFP fusion in *Dictyostelium* cells. The C-terminal tail domain was tagged with the FLAG epitope and expressed in HEK293 cells. Cell lysates from these cells were mixed and subjected to immunoprecipitation using beads coupled to anti-FLAG antibodies. Introducing the A4 mutation into full length PTEN allowed to examine interactions of the core region of $PTEN_{A4}$ and the C-terminal tail (Fig. 2E-G). We found that $PTEN_{C124S,A4}$ failed to bind to the C-terminal tail, but $PTEN_{R130G,A4}$ maintained its binding ability (Fig. 2F and G). Therefore, C124S impairs the ability of the core region to interact with the inhibitory tail, thereby stimulating membrane recruitment of PTEN.

The residue C124 can form a disulfide bond with another residue, C71, in the catalytic domain and disruption of this covalent bond has been proposed to target PTEN to the plasma membrane (9). However, we did not observe membrane recruitment of $PTEN_{C71S}$ (Fig. 2A and B). Therefore, the mechanism that recruits $PTEN_{C124S}$ is not likely the break of the C124-C71 bond. To ameliorate the effects of various mutations on stability, we analyzed PTEN in the presence of MG132 for the remainder of this study.

Since our screen isolated mutations near the C-terminal phosphorylation sites (Fig. 1A, Y379, S380, T382, T383), we compared the role of each of the four phosphorylation sites (S380, T382, T383, and S385) in membrane localization of PTEN. We found that substitutions of S380, T382 and T383 promoted membrane localization of PTEN, whereas S385 did not (Fig. 3A and B). In addition to the phosphorylation sites, the mutation Y379N greatly decreased phosphorylation of the C-terminal tail, suggesting that inhibition of phosphorylation recruits $PTEN_{Y379N}$ to the plasma membrane (Fig. 3D). Furthermore, previous studies identified three additional residues (S362, T366, and S370), which were phosphorylated at the C-terminal region. However, we found that substitutions at these residues did not affect PTEN localization (Fig. 3A and B). Finally, the phosphorylation mutations that increased membrane localization of PTEN also increased its nuclear localization (Fig. 3A-C); therefore, the mechanisms that regulate PTEN membrane and nuclear localization may be related.

Our screen also isolated previously uncharacterized mutations that increase membrane localization (Fig. 1A). First, the combination of two mutations, N262Y (located in the CBR3 loop of the C2 domain) and N329H (located in the Cα2 loop of the C2 domain), increased membrane localization of PTEN, although each mutation alone was ineffective (Fig. 4A and B). This increased membrane association was not due to decreased phosphorylation of the C-terminal domain (Fig. 4C). Second, the mutation K269E (located in the CBR3 loop), which alone did not affect membrane binding of PTEN, dramatically stimulated membrane localization in combination with the mutation D381V (located near the C-terminal phosphorylation site), which alone only slightly increased membrane localization (Fig. 4A and B). D381V decreased phosphorylation of the C-terminal tail while K269E did not affect phosphorylation (Fig. 4C). To test whether these amino acids are specifically coupled with each other, we examine the localization of $PTEN_{N262Y,\ D381V}$ and $PTEN_{K269E,\ N329H}$, $PTEN_{N262Y,\ K269E}$, and $PTEN_{N329H,\ D381V}$. All of the four mutants significantly enhanced membrane localization (Fig. 4D and E). Among them, combinations of mutations in the tail domain with either the CBR3 loop ($PTEN_{N262Y,\ D381V}$ and $PTEN_{K269E,\ D381V}$) or the Cα2 loop ($PTEN_{N329H,\ D381V}$) showed stronger effects. A combination of two mutations within the CBR3 loop showed relatively modest effects ($PTEN_{N262Y,\ K269E}$). It is likely that mutations in the C2 domain and the C-terminal tail additively stimulate membrane recruitment of PTEN.

The CBR3 loop contains five lysines, K260, K203, K266, K267, and K269, which interact with phosphatidylserine (12, 20, 21); however, their function in membrane recruitment has not been directly tested in cells. In addition, the loop is important for interactions with the C-terminal tail, as simultaneous substitution of all of the five lysine residues inhibits interactions of the core region with the tail domain (9). Our findings that $PTEN_{N262Y,N329H}$ and $PTEN_{K269E,D381V}$ increased membrane recruitment suggested that the mutations N262Y and K269E may selectively block interactions with the tail domain but not with the membrane. Therefore, we thought that the roles of the CBR3 loop in core-tail interactions and in membrane association are separable. To test this idea, we substituted five lysines to alanines simultaneously and individually. When all of the lysines were replaced with alanine ($PTEN_{CBR(K5A)}$) or aspartate ($PTEN_{CBRK(5D)}$) neither molecule localized to the plasma membrane but both showed increased nuclear localization (Fig. 4F and G). Furthermore,

$PTEN_{CBR(K5A)}$ and $PTEN_{CBR(K5D)}$ remained to be defective in membrane localization, even if the A4 mutation was introduced into them (Fig. 4H and I). However, not all of the lysines were required for membrane localization. While individual mutations at K260, K263, and K267 almost completely abolished membrane localization of $PTEN_{A4}$, a mutation at K269 only partially decreased it (Fig. 4H and I). In addition, nuclear localization was not affected by all of the individual lysine mutations in $PTEN_{A4}$ (Fig. 4H and I).

Next, we performed pull-down assays to examine the roles of the five lysines in interactions with the tail domain. $PTEN_{A4}$, but not WT PTEN, $PTEN_{CBR(K5A),A4}$, or $PTEN_{CBR(K5D),A4}$, co-immunoprecipitated with the tail domain (Fig. 4J). Individual substitution of the five lysines with alanine showed that K260A, K263A, K267A, and K269A, but not K266A, compromised interactions, with the strongest effect achieved by K269A (Fig. 4K). Thus, K260, K263, and K267 may mediate interactions with both the membrane and the tail domain, whereas K269 mainly mediates interactions with the tail and only partially with the membrane. In addition to the lysine residues, N262 within the CBR3 loop may also selectively interact with the tail domain as the combination of the mutations N262Y and N329H blocked binding of the core region and to the tail domain (Fig. 4J).

To study the function of PTEN, we examined the phosphatase activity of PTEN mutants. We immunopurified PTEN-GFP using beads coupled to anti-GFP antibodies and measured the phosphatase activity against a soluble form of PIP3, PIP3 diC8 (Fig. 5A). C124S, R130G and C124S,A4 blocked the phosphatase activity whereas CBR(K5A), CBR(K5D) and N262Y,N329H did not. Interestingly, A4 increased the phosphatase activity, suggesting that the C-terminal tail negatively regulates the activity, in addition to membrane localization. We further tested PTEN function in cells by analyzing the ability to rescue PTEN-null *Dictyostelium* cells. Upon starvation, *Dictyostelium* cells move toward cAMP, aggregate and differentiate into multicellular structures called fruiting bodies which consist of spore and stalk cells (Fig. 5B, WT) (22). PTEN is necessary for chemotactic migration toward cAMP and PTEN-null cells are defective in aggregation and differentiation (Fig. 5B, vector) (14). $PTEN_{A4}$, $PTEN_{K269E,\ D381D}$, and $PTEN_{N262Y,329H}$ reversed the developmental defects in the PTEN-null *Dictyostelium* cells, whereas $PTEN_{C124S}$, $PTEN_{C124S,\ A4}$, $PTEN_{CBR3(K5A)}$, and $PTEN_{CBR3(K5D)}$ did not (Fig. 5B). However, the inability of $PTEN_{CBR3(K5A)}$ and $PTEN_{CBR3(K5D)}$ to rescue the PTEN-null phenotype was not due to the lack of the phosphatase activity (Fig. 5A). Moreover, when we examined the effect of substitution of the five lysine residues in the CBR3 loop, K260A and K263A, which blocked membrane association, failed to rescue the developmental defects in PTEN-null cells while K266A, K267A and K269A partially rescued the phenotype (Fig. 5C), similar to their effects on the membrane association of $PTEN_{A4}$ (Fig. 5C and D). Therefore, our findings suggest that membrane recruitment is necessary for PTEN function.

Finally, we validated our findings made in *Dictyostelium* cells by expressing WT and mutant forms of PTEN-GFP in HEK293T cells (Fig. 6). While WT PTEN is mainly located in the cytosol, $PTEN_{C124C}$ and $PTEN_{A4}$ increased association with the plasma membrane, consistent with previous reports. Combination of C124 and A4 further recruited $PTEN_{C124S,A4}$ to the membrane. Moreover, the new substitutions that we isolated in this

study (K269E, D381V and N262Y, N329H) promoted membrane localization of PTEN in HEK293T cells, as observed in *Dictyostelium* cells.

Discussion

In this study, we showed that heterologous expression in *Dictyostelium* cells enabled a rapid visual inspection of PTEN localization in single colonies with efficient recovery of plasmids to identify mutations by DNA sequencing. Expression of human PTEN in *Dictyostelium* cells allows improved visualization of membrane localization relative to mammalian cells, a simple readout of overall function, and the ability to carry out random mutagenesis. With this system, we have defined mechanisms that control membrane localization of human PTEN. Furthermore, taking advantage of the fact that human PTEN functionally replaces *Dictyostelium* PTEN, we demonstrated the functional importance of membrane recruitment of human PTEN in cells.

Based on our findings, we propose that the CBR3 loop, the C2 loop, and the catalytic domain form a membrane-binding regulatory interface at one surface of the PTEN protein (Fig. 7). Supporting our model, the membrane-binding regulatory interface can be seen in the crystal structure of the PTEN molecule (Fig. 1A). The three lysines at residues 260, 263, and 267 in the CBR3 loop are critical for the membrane association and function of PTEN in cells. These positively-charged residues may directly form a bridge with negatively-charged phospholipid head groups in the plasma membrane (Fig. 7). Consistent with this model, a previous biochemical study showed that the CBR3 loop is necessary for interactions of PTEN with phosphatidylserine (12, 20, 21).

The CBR3 loop is also important for interaction with the inhibitory C-terminal tail domain (Fig. 7). Thus, the positively-charged CBR3 loop may bind to phosphates at residues S380 and T383 in the tail domain. Previous studies have suggested that in this “closed” form of the enzyme, the membrane-binding capacity is blocked by steric hindrance. We show that the Cα2 loop, which contains the residue N329, and the catalytic domain do not appear to directly interact with the membrane. Instead, these regions strengthen interactions with the C-terminal tail. Similarly, the lysine at 269 in the CBR3 loop appears to mainly mediate interactions with the tail domain but not with the membrane. The C-terminal tail domain dissociates from the CBR3 loop upon dephosphorylation, allowing the face of the protein including the CR3 loop to bind to the membrane. The C-terminal tail can not only block membrane association, it can also inhibit enzymatic activity, as $PTEN_{A4}$ had higher phosphatase activity. Our model envisions that opening the conformation of PTEN provides its robust activation by releasing the inhibitory effects of the tail domain on both its localization and activity.

It has been shown that interactions of the C-terminal tail with the core region are important for the stability of PTEN (18). Our current study supports this model and further shows that $PTEN_{A4}$ is degraded by proteosomes and this degradation requires its phosphatase activity. We speculate that phosphorylation of PTEN may inhibit this mechanism while auto-dephosphorylation by PTEN may release this inhibition and stimulate degradation of PTEN by protesomes. It is currently unknown which phosphorylated residues mediate this

regulation. It is also possible that PTEN degradation is coupled to its enzymatic action at the plasma membrane. This coupling could potentially serve as a clock that determines the timeframe in which PTEN is active at the membrane, which would help sustain intracellular PIP3 signaling. It would be interesting to speculate that this degradation mechanism is modified by phosphatidylinositol in the plasma membrane, providing feedback from the level of PIP3 and/or PIP2. Interactions with these phosphatidylinositols may control the conformation of PTEN and target PTEN for degradation. Finally, nuclear localization of PTEN may help protect PTEN from degradation by sequestering the protein from the degradation machinery at the membrane.

Materials and Methods

Cell culture and plasmids

All *Dictyostelium* cells were cultured in HL5 medium at 22°C. Cells expressing PTEN-GFP were selected by G418 (20 μg/ml). LY294002 (20 μM), MG132 (20 μM) and cycloheximide (40 μg/ml) were used to inhibit PI3K, proteasomes and protein synthesis, respectively. The PCR primers and plasmids used in this study are listed in Tables S1 and S2, respectively. Human PTEN was mutagenized using overlap extension PCR as previously described (23) and cloned into pKF3, a *Dictyostelium* expressing plasmid carrying GFP. All constructs were confirmed by DNA sequencing. HEK293T cells were maintained in DMEM (Invitrogen) supplemented with 10 % FBS (Invitrogen). Cells were transiently transfected with 1 μg of DNA plasmids on eight-well chambered coverglass (Lab-TekII, Nunc) using 3 μl of GeneJuice (Novagen), following the manufacturer's protocol. Cells were then incubated for 24 hours before observation.

Isolation of PTEN mutants that show enhanced membrane localization

Human PTEN cDNA was randomly mutagenized using a Diversity PCR random mutagenesis kit (Clontech). The PCR products were cloned into the pKF3 plasmid and electroporated into MegaX DH10B competent cells (Invitrogen). More than 120,000 bacterial colonies were collected. Ten of the mutagenized plasmids were sequenced to check distribution and diversity of mutations. The extracted plasmids were pooled to create the PTEN library and electroporated into *Dictyostelium* cells (14, 24). More than 20,000 transformants were collected and cultured under shaking condition in the presence of G418 for 5 days. Cells were plated on five 96-well optical plates (Thermo Scientific) at a density of 1,000 cells/well. After 3 days, cells with increased membrane localization of PTEN-GFP were manually picked up by a pipette under a Zeiss HAL100 epifluorescence inverted microscope equipped with a 40X objective and transferred to new wells. This isolation process was repeated until cells with increased membrane localization of PTEN comprise about 50-70% of the total cell population in each well. To isolate individual clones, cells were plated on SM agar with *K. aerogenes*. After 5 days, individual plaques from SM plates were transferred to the optical plate and confirmed for enhancement of membrane association of PTEN-GFP. To identify mutations that resulted in increased membrane localization, the PTEN gene isolated from individual clones was PCR-amplified and sequenced. To identify mutations that are responsible for enhanced membrane localization, mutations were separated by subcloning a DNA fragment of the PTEN gene. In some cases,

single mutations were created in the PTEN gene using site-directed mutagenesis with overlap extension PCR.

Confocal microscopy and quantification of PTEN-GFP localization

To observe PTEN-GFP, cells were washed with DB and placed on eight-well chambered coverglass (Lab-TekII, Nunc). Fluorescent images were acquired under a Leica DMI 6000 inverted microscope equipped with a 63x objective and captured by a CoolSNAP EZ camera. All images were analyzed using Image J software. To quantify fluorescence intensity of PTEN-GFP at the plasma membrane and nucleus relative to the cytosol, we measured and averaged fluorescence intensity in 1 pixel area from three different positions in each compartment. Background fluorescence intensity was subtracted from each measurement. The nucleus was identified by DAPI staining. To integrate fluorescence intensity of PTEN-GFP at the plasma membrane, the total intensity at the cell periphery was measured and normalized relative to that in the cytotol.

Developmental assay

PTEN-null *Dictyostelium* cells were grown exponentially (4×10^5 cells/ml), washed twice in DB (10 mM phosphate buffer, 2 mM $MgSO_4$, 0.2 mM $CaCl_2$), and plated on 1% non-nutrient DB agar for 36 hours (25, 26). Cells were observed under an Olympus SZ-PT dissecting microscope equipped with 6x objective and their images were taken by a Nikon 4500 camera.

Assays for interactions between PTEN and its C-terminal tail

Interactions between PTEN and its C-terminal tail ($PTEN_{352-403}$-YFP-FLAG) were examined, as described (9). HEK293T cells were cultured in DMEM supplemented with 10% FBS on a 100-mm dish, transiently transfected with 8 μg of the plasmid carrying $PTEN_{352-403}$-YFP-FLAG using GeneJuice (Novagen) and then cultured for 24 hours in DMEM with 10% FBS. HEK293T cells were lysed in 1 ml of lysis buffer containing 1% Nonidet P-40, 50 mM NaCl, 20 mM Tris-HCl (pH 7.5), 10% glycerol, 0.1 mM EDTA, phosphatase inhibitor cocktail (Sigma) and protease inhibitor cocktail (Roche). The lysates were then cleared by centrifugation at 13,000 rpm for 20 min at 4°C. *Dictyostelium* cells expressing WT and mutant versions of PTEN-GFP were lysed in 1% Nonidet P-40, 300 mM NaCl, 10 mM Tris-HCl (pH 7.5), 2 mM EDTA, phosphatase inhibitor cocktail (Sigma) and protease inhibitor cocktail (Roche). The lysates were then cleared by centrifugation at 13,000 rpm for 20 min at 4°C. 100 μl of the HEK293T lysates were mixed with 500 μl of the *Dictyostelium* lysates. Beads coupled to anti-FLAG antibodies (Sigma) were added to the mixtures and incubated for 2 hours. The beads were washed twice in the lysis buffer and the bound fractions were analyzed by SDS-PAGE and immunoblotting using antibodies to FLAG and GFP.

Immunoblotting

Proteins were resolved by SDS-PAGE and transferred onto PVDF membrane. Antibodies against PTEN (138G6, Cell Signaling), phosphorylated PTEN at residues S380, T382 and T383 (44A7, Cell Signaling), GFP (11E5, Molecular Probes) and actin (C-11, Santa Cruz

Biotechnology) were used. Immunocomplexes were visualized by fluorophore-conjugated secondary antibodies including anti-rabbit Alexa Fluoro 488 (Invitrogen), anti-goat Aelxa Fluoro 647 (Invitrogen) and anti-mouse Dylight 649 (Jackson ImmunoResearch Lab) and detected using a PharosFX Plus molecular imager (Bio-Rad).

In vitro phosphatase activity assay

The phosphatase activity of PTEN was measured, as described previously (17). WT and mutant forms of PTEN fused to GFP were expressed in *Dicyostelium* cells and immunopurified using GFP-Trap agarose beads (Allele Biotech). The phosphatase activity was determined by measuring release of phosphates from PIP3 diC8 using a Malachite Green Phosphatase assay kit (Echelon). The activity was normalized to amounts of purified PTEN-GFP proteins.

Statistical analysis

P values were determined using the Student's t-test: $*p< 0.05$; $**p< 0.01$; $***p< 0.001$.

Supplementary Material

Refer to Web version on PubMed Central for supplementary material.

Acknowledgements

This work was supported by NIH grants to MI (GM084015), PND (GM28007 and GM34933) and HS (GM089853 and NS084154). We thank M. Rahdar and K.F. Swaney for providing plasmids.

References

1. Hollander MC, Blumenthal GM, Dennis PA. PTEN loss in the continuum of common cancers, rare syndromes and mouse models. Nat Rev Cancer. 2011; 11(4):289–301. Epub 2011/03/25. [PubMed: 21430697]
2. Carracedo A, Alimonti A, Pandolfi PP. PTEN level in tumor suppression: how much is too little? Cancer Res. 2011; 71(3):629–33. Epub 2011/01/27. [PubMed: 21266353]
3. Leslie NR, Dixon MJ, Schenning M, Gray A, Batty IH. Distinct inactivation of PI3K signalling by PTEN and 5-phosphatases. Adv Biol Regul. 2012; 52(1):205–13. Epub 2011/09/21. [PubMed: 21930147]
4. Rodon J, Dienstmann R, Serra V, Tabernero J. Development of PI3K inhibitors: lessons learned from early clinical trials. Nat Rev Clin Oncol. 2013; 10(3):143–53. Epub 2013/02/13. [PubMed: 23400000]
5. Vanhaesebroeck B, Stephens L, Hawkins P. PI3K signalling: the path to discovery and understanding. Nature reviews Molecular cell biology. 2012; 13(3):195–203. Epub 2012/02/24.
6. Baker SJ. PTEN enters the nuclear age. Cell. 2007; 128(1):25–8. Epub 2007/01/16. [PubMed: 17218252]
7. Song MS, Salmena L, Pandolfi PP. The functions and regulation of the PTEN tumour suppressor. Nature reviews Molecular cell biology. 2012; 13(5):283–96. Epub 2012/04/05. [PubMed: 22473468]
8. Tamguney T, Stokoe D. New insights into PTEN. Journal of cell science. 2007; 120(Pt 23):4071–9. Epub 2007/11/23. [PubMed: 18032782]
9. Rahdar M, Inoue T, Meyer T, Zhang J, Vazquez F, Devreotes PN. A phosphorylation-dependent intramolecular interaction regulates the membrane association and activity of the tumor suppressor PTEN. Proc Natl Acad Sci U S A. 2009; 106(2):480–5. [PubMed: 19114656]

10. Walker SM, Leslie NR, Perera NM, Batty IH, Downes CP. The tumour-suppressor function of PTEN requires an N-terminal lipid-binding motif. The Biochemical journal. 2004; 379(Pt 2):301–7. Epub 2004/01/09. [PubMed: 14711368]
11. Denning G, Jean-Joseph B, Prince C, Durden DL, Vogt PK. A short N-terminal sequence of PTEN controls cytoplasmic localization and is required for suppression of cell growth. Oncogene. 2007; 26(27):3930–40. Epub 2007/01/11. [PubMed: 17213812]
12. Lee JO, Yang H, Georgescu MM, Di Cristofano A, Maehama T, Shi Y, et al. Crystal structure of the PTEN tumor suppressor: implications for its phosphoinositide phosphatase activity and membrane association. Cell. 1999; 99(3):323–34. Epub 1999/11/11. [PubMed: 10555148]
13. Das S, Dixon JE, Cho W. Membrane-binding and activation mechanism of PTEN. Proceedings of the National Academy of Sciences of the United States of America. 2003; 100(13):7491–6. Epub 2003/06/17. [PubMed: 12808147]
14. Iijima M, Devreotes P. Tumor suppressor PTEN mediates sensing of chemoattractant gradients. Cell. 2002; 109(5):599–610. [PubMed: 12062103]
15. Vazquez F, Matsuoka S, Sellers WR, Yanagida T, Ueda M, Devreotes PN. Tumor suppressor PTEN acts through dynamic interaction with the plasma membrane. Proceedings of the National Academy of Sciences of the United States of America. 2006; 103(10):3633–8. Epub 2006/03/16. [PubMed: 16537447]
16. Iijima M, Huang YE, Devreotes P. Temporal and spatial regulation of chemotaxis. Dev Cell. 2002; 3(4):469–78. [PubMed: 12408799]
17. Iijima M, Huang YE, Luo HR, Vazquez F, Devreotes PN. Novel mechanism of PTEN regulation by its phosphatidylinositol 4,5-bisphosphate binding motif is critical for chemotaxis. J Biol Chem. 2004; 279(16):16606–13. [PubMed: 14764604]
18. Vazquez F, Ramaswamy S, Nakamura N, Sellers WR. Phosphorylation of the PTEN tail regulates protein stability and function. Molecular and cellular biology. 2000; 20(14):5010–8. Epub 2000/06/24. [PubMed: 10866658]
19. Myers MP, Pass I, Batty IH, Van der Kaay J, Stolarov JP, Hemmings BA, et al. The lipid phosphatase activity of PTEN is critical for its tumor supressor function. Proceedings of the National Academy of Sciences of the United States of America. 1998; 95(23):13513–8. Epub 1998/11/13. [PubMed: 9811831]
20. Shenoy S, Shekhar P, Heinrich F, Daou MC, Gericke A, Ross AH, et al. Membrane association of the PTEN tumor suppressor: molecular details of the protein-membrane complex from SPR binding studies and neutron reflection. PLoS One. 2012; 7(4):e32591. Epub 2012/04/17. [PubMed: 22505997]
21. Lumb CN, Sansom MS. Defining the membrane-associated state of the PTEN tumor suppressor protein. Biophysical journal. 2013; 104(3):613–21. Epub 2013/02/28. [PubMed: 23442912]
22. Fey P, Kowal AS, Gaudet P, Pilcher KE, Chisholm RL. Protocols for growth and development of Dictyostelium discoideum. Nat Protoc. 2007; 2(6):1307–16. [PubMed: 17545967]
23. Zhang P, Wang Y, Sesaki H, Iijima M. Proteomic identification of phosphatidylinositol (3,4,5) triphosphate-binding proteins in Dictyostelium discoideum. Proc Natl Acad Sci U S A. 2010
24. Chen CL, Wang Y, Sesaki H, Iijima M. Myosin I Links PIP3 Signaling to Remodeling of the Actin Cytoskeleton in Chemotaxis. Science signaling. 2012; 5(209):ra10. Epub 2012/02/03. [PubMed: 22296834]
25. Cai H, Huang CH, Devreotes PN, Iijima M. Analysis of chemotaxis in Dictyostelium. Methods in molecular biology. 2012; 757:451–68. Epub 2011/09/13. [PubMed: 21909927]
26. Wang Y, Steimle PA, Ren Y, Ross CA, Robinson DN, Egelhoff TT, et al. Dictyostelium huntingtin controls chemotaxis and cytokinesis through the regulation of myosin II phosphorylation. Mol Biol Cell. 2011; 22(13):2270–81. [PubMed: 21562226]

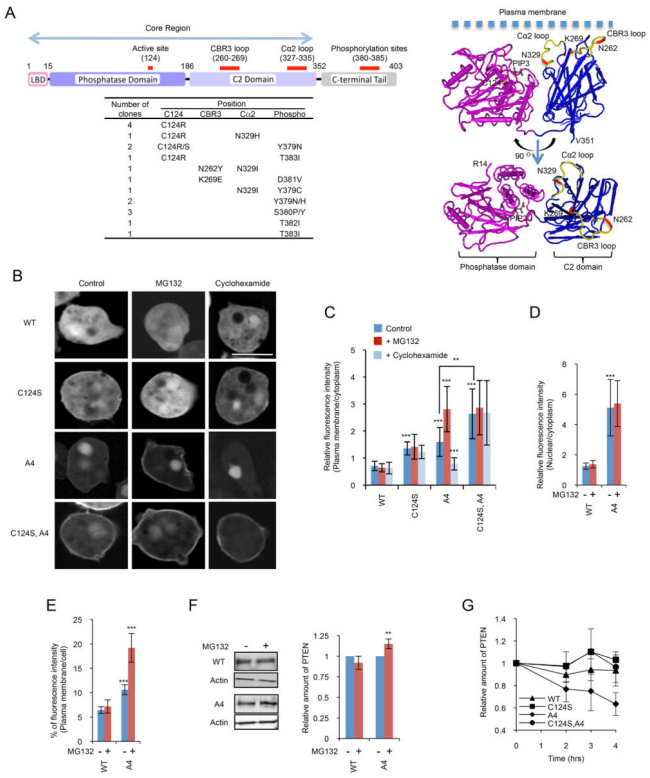

Figure 1. Isolated PTEN mutations

(A) The domain structure of PTEN is shown. The table summarizes the position and frequency of mutations isolated in the screen. The isolated mutations were indicated in the 3-D structure of PTEN with the phosphatase and C2 domains (R14-V351) (12) (http://www.ncbi.nlm.nih.gov/Structure/mmdb/mmdbsrv.cgi?uid=11638). (B) *Dictyostelium* cells expressing GFP fused to PTEN, $PTEN_{C124S}$, $PTEN_{A4}$, and $PTEN_{C124S,A4}$ were viewed by fluorescence microscopy. Cells were incubated in the presence or absence of 20 μM MG132 or 40 μg/ml cycloheximide. Bar, 10 μm. (C and D) Fluorescence intensity of GFP fused to WT or the indicated PTEN mutant at the plasma membrane (C) or nucleus (D) was quantified relative to that in the cytosol as described in Materials and Methods. Values represent the mean ± SD ($n \geq 15$). (E) Integrated fluorescence intensity of PTEN-GFP and $PTEN_{A4}$-GFP at the plasma membrane was normalized relative to total fluorescence intensity in cells ($n \geq 10$). (F) Whole-cell lysates prepared from cells expressing PTEN-GFP or $PTEN_{A4}$-GFP were analyzed by immunoblotting with antibodies against GFP and actin in the presence or absence of MG132. Band intensity was quantified ($n = 3$). (G) Cells expressing GFP fused to the indicated forms of PTEN were incubated with 40 μg/ml cycloheximide. Whole-cell lysates were analyzed by immunoblotting with anti-GFP antibodies at the indicated time points. Band intensity was quantified relative to 0 hour sample ($n = 3$).

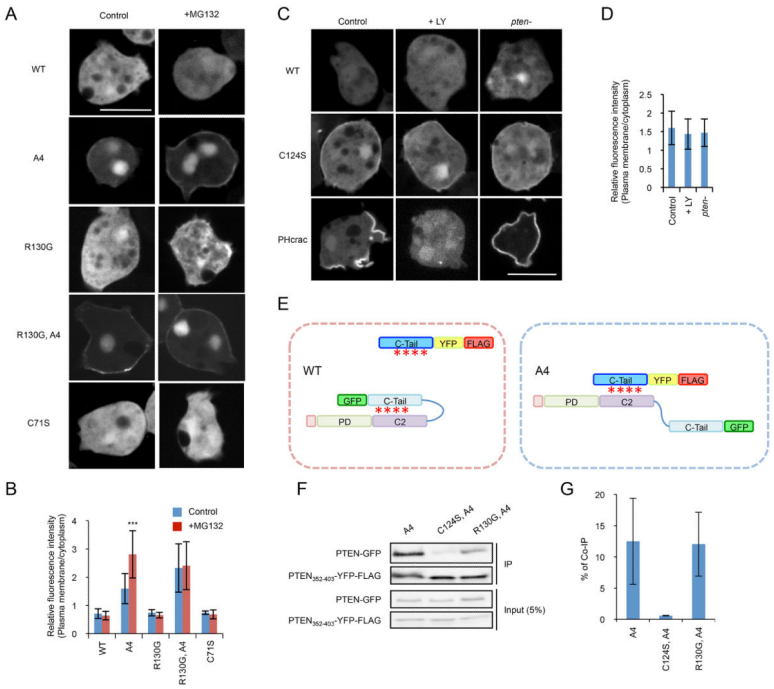

Figure 2. Analysis of PTEN$_{C124S}$

(A) *Dictyostelium* cells expressing GFP fused to PTEN, PTEN$_{A4}$, PTEN$_{R130G}$, PTEN$_{R130G, A4}$, and PTEN$_{C71S}$ were incubated with 20 μM MG132 for 6 hour and viewed by fluorescence microscopy. Bar, 10 μm. (B) Fluorescence intensity at the plasma membrane was quantified ($n \geq 15$). (C and D) WT and PTEN-null cells expressing PTEN-GFP, PTEN$_{C124S}$-GFP or PHcrac-GFP were observed by fluorescence microscopy in the presence or absence of 20 μM LY294002. Fluorescence intensity of PTEN$_{C124S}$-GFP at the plasma membrane was quantified (D). Values represent the mean ± SD ($n \geq 15$). (E-G) Interaction of the C-terminal tail domain of PTEN with full length PTEN was assessed by pull-down assay. Whole-cell lysates expressing PTEN-GFP, PTEN$_{C124S,A4}$-GFP, or PTEN$_{R130G,A4}$-GFP were incubated with PTEN$_{352–403}$-YFP-FLAG. Introducing the A4 mutation into full length PTEN allowed to examine interactions of the core region of PTEN$_{A4}$ and the C-terminal tail, as shown in (E). PTEN$_{352–403}$-YFP-FLAG was immunoprecipitated with beads coupled to anti-FLAG antibodies. Bound fractions (immunoprecipitates, IP) were analyzed with antibodies to GFP and FLAG. (G) Band intensity was quantified ($n = 3$).

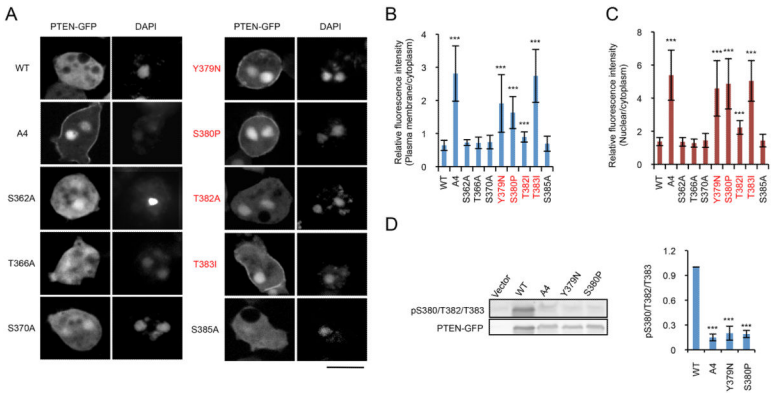

Figure 3. Mutational analysis of the C-terminal phosphorylation sites of PTEN

(A-C) *Dictyostelium* cells expressing GFP fused to the indicated version of PTEN were observed by fluorescence microscopy in the presence of 20 μM MG132 (A). Bar, 10 μm. GFP intensities at the plasma membrane (B) and nucleus (C) were determined relative to that in the cytosol. Values represent the mean ± SD ($n \geq 15$). The mutations isolated from our screen are shown in red. (D) Whole-cell lysates expressing the indicated forms of PTEN-GFP were analyzed by immunoblotting with antibodies against phospho-PTEN (pS380/T382/T383) and GFP (PTEN-GFP). Band intensity was quantified ($n \geq 3$).

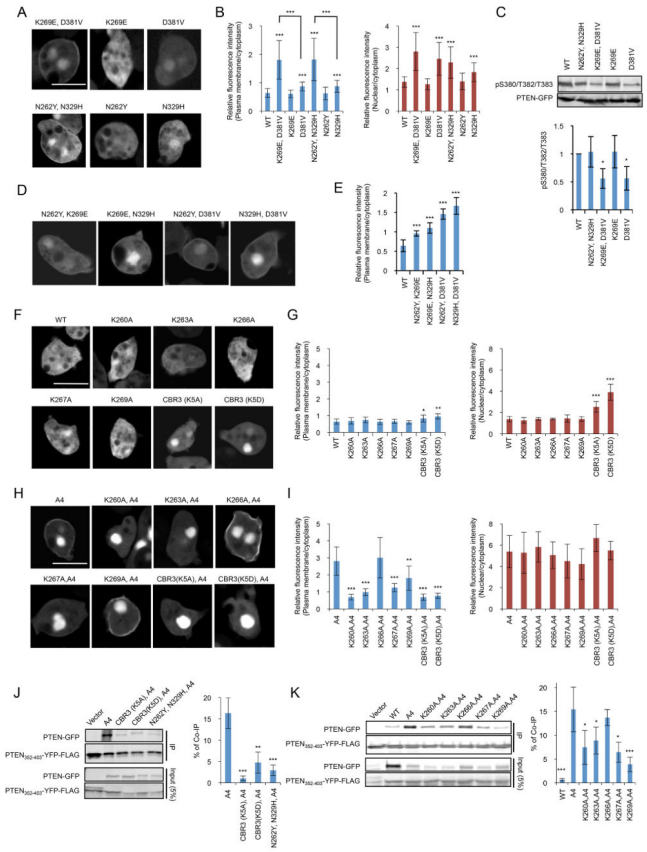

Figure 4. The CBR3 and Cα2 loops are important for interactions with the plasma membrane and the C-terminal tail

(A and B) *Dictyostelium* cells expressing the indicated forms of PTEN-GFP were viewed by fluorescence microscopy in the presence of 20 μM MG132 (A). Intensities of GFP signals at the plasma membrane and nucleus were quantified relative to that in the cytosol (B). Bar, 10 μm. (C) Whole-cell lysates expressing GFP fused to different forms of PTEN were analyzed by immunoblotting with antibodies against phospho-PTEN (pS380/T382/T383) and GFP (PTEN-GFP). Band intensity was quantified ($n \geq 3$).(D and E) Cells expressing the indicated versions of PTEN-GFP were examined in the presence of 20 μM MG132 (D). Fluorescence intensity of GFP at the plasma membrane was quantified (E). Values represent the mean ± SD ($n \geq 15$). (F and G) GFP fused to PTEN with the indicated mutations in the CBR3 loop were expressed in *Dictyostelium* cells in the presence of 10 μM MG132 (F). Relative GFP signals at the plasma membrane and nucleus were determined relative to that in the cytosol (G). (H and I) GFP fused to $PTEN_{A4}$ with the indicated CBR3 loop mutations were expressed in *Dictyostelium* cells in the presence of 20 μM MG132 (H). Relative GFP signals at the plasma membrane and nucleus were determined relative to that in the cytosol (I). (J and K) Interaction of the C-terminal domain of PTEN carrying mutations in the CBR3 and Cα2 loops with its N-terminal core region was assessed in pull-down assays. $PTEN_{352–403}$-YFP-FLAG was added to whole-cell lysates expressing the indicated PTEN-GFP constructs and immunoprecipitated with beads coupled to anti-FLAG antibodies. Bound fractions (IP) were analyzed with antibodies to GFP and FLAG. Band intensity was quantified ($n = 3$).

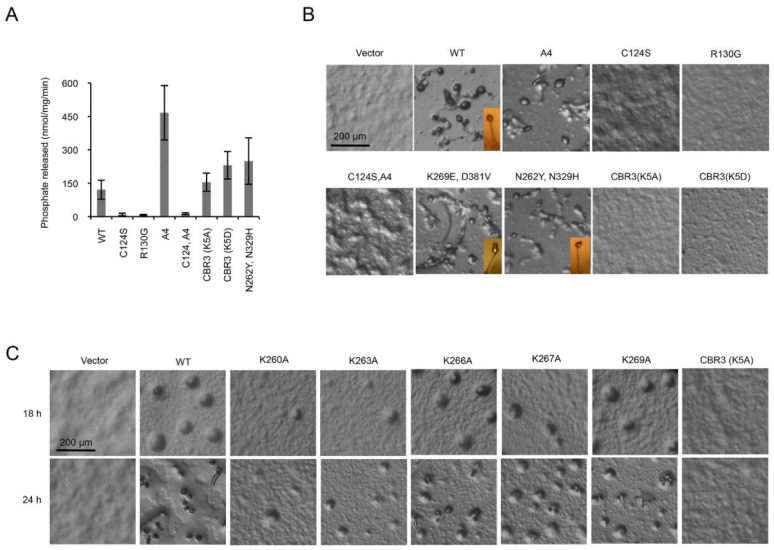

Figure 5. PTEN requires membrane association and phosphatase activity for its function

(A) The indicated PTEN-GFP proteins were immunopurified from *Dictyostelium* cells, and phosphatase activities were measured ($n \geq 3$). (B and C) PTEN-null *Dictyostelium* cells expressing different PTEN-GFP constructs were starved to induce differentiation into fruiting bodies. Pictures were taken at 36 hours (B) and 18 and 22 hours (C) after the onset of starvation. While PTEN-null cells expressing PTEN (WT) formed fruiting bodies, PTEN-null cells expressing a vector alone did not aggregate and remained undifferentiated (B). Inserts show side views of fruiting bodies (B).

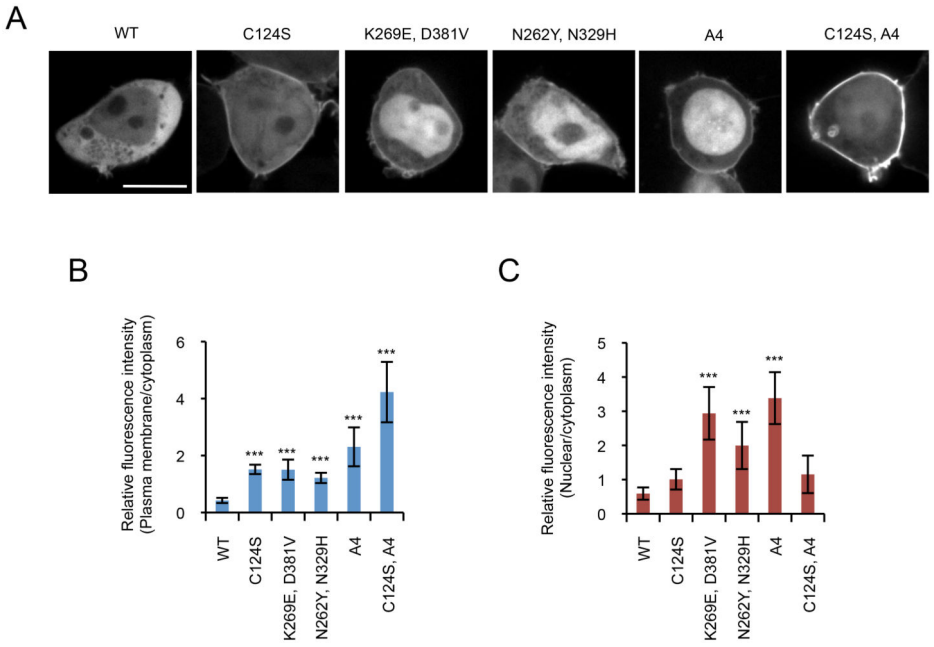

Figure 6. Localization of GFP-PTEN in HEK293T cells

HEK293T cells expressing the indicated forms of PTEN-GFP were viewed by fluorescence microscopy (A). (B and C) Intensities of GFP signals at the plasma membrane (B) and nucleus (C) were quantified relative to that in the cytosol (B). Bar, 10 μm.

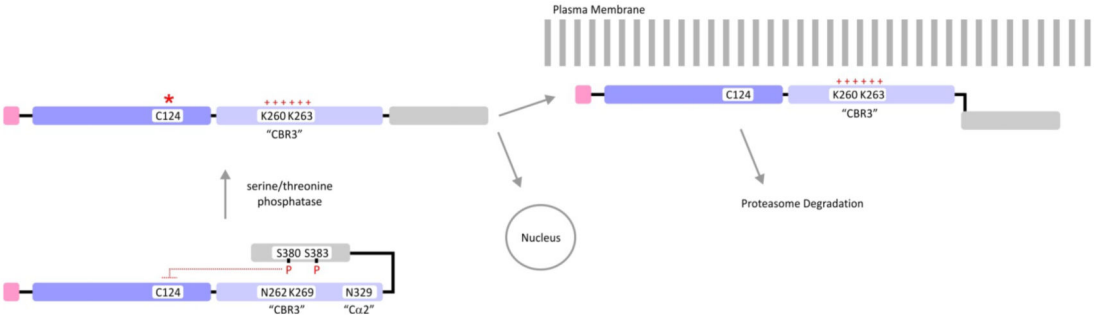

Figure 7. Model for mechanisms of PTEN membrane localization

Positively-charged lysine residues (K260, K263, and K269) in the CBR3 loop are masked by phosphorylated serine (S380) and threonine (T383) in the C-terminal tail. PTEN adopts an open conformation upon dephosphorylation of the tail, and the two lysine residues interact with negatively-charged phospholipids in the plasma membrane. Proteasome-mediated degradation of PTEN occurs rapidly at the plasma membrane and is dependent upon the phosphatase activity of PTEN. The open conformation of dephosphorylated PTEN would also expose an otherwise hidden nuclear localization signal to promote nuclear import of PTEN.